ENGINEERING

Rubbery electronics and sensors from intrinsically stretchable elastomeric composites of semiconductors and conductors

Hae-Jin Kim,[1] Kyoseung Sim,[2] Anish Thukral,[1] Cunjiang Yu[1,2,3,4]*

A general strategy to impart mechanical stretchability to stretchable electronics involves engineering materials into special architectures to accommodate or eliminate the mechanical strain in nonstretchable electronic materials while stretched. We introduce an all solution–processed type of electronics and sensors that are rubbery and intrinsically stretchable as an outcome from all the elastomeric materials in percolated composite formats with P3HT-NFs [poly(3-hexylthiophene-2,5-diyl) nanofibrils] and AuNP-AgNW (Au nanoparticles with conformally coated silver nanowires) in PDMS (polydimethylsiloxane). The fabricated thin-film transistors retain their electrical performances by more than 55% upon 50% stretching and exhibit one of the highest P3HT-based field-effect mobilities of 1.4 $cm^2/V{\cdot}s$, owing to crystallinity improvement. Rubbery sensors, which include strain, pressure, and temperature sensors, show reliable sensing capabilities and are exploited as smart skins that enable gesture translation for sign language alphabet and haptic sensing for robotics to illustrate one of the applications of the sensors.

INTRODUCTION

The past decade has witnessed significant advancements in stretchable electronics. Owing to its superior mechanical characteristics (that is, soft, bendable, stretchable, and twistable), stretchable electronics hold promise in health monitors (*1*, *2*), medical implants (*3*–*5*), artificial skins (*6*–*8*), and human-machine interfaces (*9*, *10*). To date, most electronic materials, especially semiconductors, including inorganics (such as Si and GaAs) and organics [such as poly(3-hexylthiophene-2,5-diyl) (P3HT) and pentacene], are mechanically nonstretchable (*11*, *12*). To enable mechanical stretchability in electronic devices, special mechanical structures or architectures have generally been used to accommodate or eliminate mechanical strain in nonstretchable materials while stretched. Examples of these structures include out-of-plane wrinkles (*13*), in-plane serpentines (*14*), rigid islands with deformable interconnects (*15*, *16*), and kirigami architectures (*17*–*19*). An alternative route to eliminating the burden of constructing dedicated architectures and the associated sophisticated fabrication processes is to build stretchable electronics from intrinsically stretchable electronic materials, which have potential toward scalable manufacturing, high-density device integration, large strain tolerance, and low cost (*11*, *20*). Although conductors that are intrinsically stretchable have been reported extensively (*21*), semiconductors that are intrinsically stretchable have been a general challenge. Existing ways of improving stretchability in semiconductors include using conjugated polymer nanowire and nanofibril networks (*22*–*24*) and microcracked films (*25*). However, their mobilities are generally very low. Recently, stretchable polymer semiconductors with relatively high mobilities and the associated thin-film transistors (TFTs) have been successfully demonstrated from dedicated polymer and nanostructure designs (*26*, *27*).

Here, we report highly stretchable electronics and sensors that are made of intrinsically stretchable composite semiconductors and conductors. Specifically, we exploit P3HT nanofibril (P3HT-NF) percolated polydimethylsiloxane (PDMS) rubber composite as a stretchable semiconductor, Au nanoparticles with conformally coated silver nanowires (AuNP-AgNW) dispersed within PDMS as a stretchable conductor, and ion gel as a gate dielectric. In particular, instead of creating novel polymers for stretchable semiconductors, which heavily require sophisticated molecular design and synthesis, we use all commercially available materials as precursors to achieve highly stretchable semiconductors that can be manufactured in a repeatable and scalable manner and have stable performances. The P3HT-NF percolated PDMS rubber composite maintains semiconductor characteristics under 50% mechanical stretching along and perpendicular to the channel length directions. Simple solution processes are used to form thin films to construct stretchable devices, including TFTs and sensors, without any additional structural design to achieve large mechanical stretchability. Examples of intrinsically stretchable electronics that have been exploited include stretchable ion gel–gated TFTs and strain, pressure, and temperature sensors. The ion gel–gated TFTs exhibited a field-effect mobility (μ_{FE}) and an on/off ratio ($I_{ON/OFF}$) of 1.4 $cm^2/V{\cdot}s$ and 5.6×10^3, respectively. While the mobility achieved a high value for the stretchable organic format of semiconductors, it only has a moderate decrease of less than 45% under 50% mechanical stretching. We demonstrate the application of these intrinsically stretchable electronics as multifunctional artificial robotic skins that can translate hand motions and gestures to provide haptic sensing capabilities.

RESULTS

Intrinsically stretchable elastomeric composite conductors and semiconductors

Figure 1A shows a schematic illustration of sensors (upper) and TFTs (lower), which were constructed from AuNP-AgNW/PDMS elastomeric conductor, P3HT-NF/PDMS elastomeric semiconductor, and ion gel dielectric. We used AuNP-AgNW/PDMS composites as stretchable conductors to form an ohmic contact with P3HT-NF/PDMS because an energy barrier would exist for AgNW-based electrodes (*28*). We coated the AgNWs with AuNPs using a galvanic replacement process

[1]Department of Mechanical Engineering, University of Houston, Houston, TX 77204, USA. [2]Materials Science and Engineering Program, University of Houston, Houston, TX 77204, USA. [3]Department of Electrical and Computer Engineering, University of Houston, Houston, TX 77204, USA. [4]Department of Biomedical Engineering, University of Houston, Houston, TX 77204, USA.
*Corresponding author. Email: cyu15@uh.edu

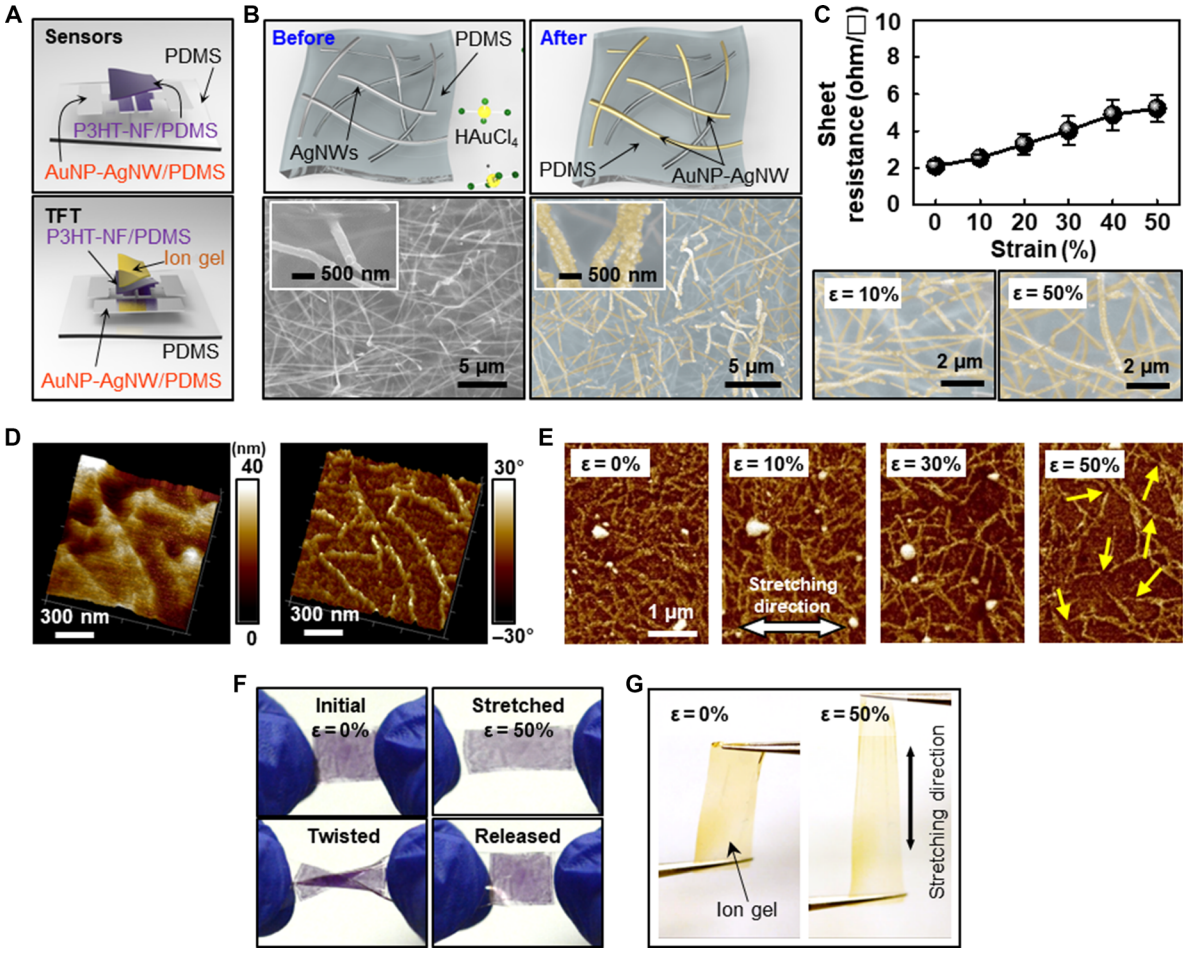

Fig. 1. Intrinsically stretchable electronic materials. (**A**) Schematic illustrations of a sensor (upper) and a TFT (lower), consisting of AuNP-AgNW conductors, P3HT-NF/PDMS semiconductor composite, and ion gel dielectric vertically stacked on a PDMS substrate. (**B**) Schematic illustrations (upper) and SEM images (lower) of the AgNWs before (left) and after (right) the galvanic replacement process to conformally coat AuNPs on exposed AgNWs. (**C**) Sheet resistance (ohms/□) of the AuNP-AgNW/PDMS conductor under different levels of mechanical strain. The SEM images of the stretched conductor are shown at the bottom. (**D**) AFM surface topography (left) and phase mode (right) images of the P3HT-NF/PDMS film. (**E**) AFM phase mode images of P3HT-NF/PDMS coated on a PDMS substrate upon uniaxial stretching. Yellow arrows indicate P3HT-NF rupture. (**F**) Photographs of the P3HT-NF/PDMS film on a thin PDMS substrate under various forms of mechanical deformation. (**G**) Photographs of free-standing ion gel dielectric before and after stretching.

to form AuNP-AgNW (*29*). Comparison studies in transistor characteristics are described to further emphasize the necessity of developing these conductors. The detailed electrode preparation process is presented in Materials and Methods. Figure 1B shows the schematic illustrations of the AgNW before (upper left) and after (upper right) AuNP conformal coating. Note that only the exposed AgNWs will be coated with AuNPs. Scanning electron microscopy (SEM) images of AgNWs before (bottom left) and after (bottom right) conformal AuNP coating indicate the success of the galvanic replacement process (fig. S1). We performed stretching tests to examine the electrical characteristic change associated with the applied mechanical strain. Specifically, the AuNP-AgNW/PDMS electrode can be elastically stretched, and its sheet resistance increases from 2 to 5 ohms/□ upon 50% uniaxial stretching, as shown in Fig. 1C (upper). The SEM images in Fig. 1C (lower) revealed that no obvious crack was observed.

The stretchable elastomeric composite semiconductor is prepared by two major sequential steps: (i) forming the one-dimensional self-assembled π-conjugated P3HT-NFs in the solvent under a cooling process and (ii) blending the resulting P3HT-NFs with PDMS to yield percolated nanofibrils in a rubber matrix. This process not only forms percolated pathways for the carriers to transport but also results in P3HT-NFs that significantly improve crystallinity and therefore enhance the carrier mobility, as detailed in previous studies (*22*, *23*, *30*). Specifically, P3HT was first dissolved in the *m*-xylene solvent at 60°C (fig. S2A, bright orange) and then cooled down and kept for 10 min at −20°C to form P3HT-NF (fig. S2A, dark purple). Transmission electron microscopy (TEM) and atomic force microscopy (AFM) images of the prepared P3HT-NF indicate that the diameter and length of P3HT-NF are 40 nm and 1.5 μm, respectively (fig. S2). The P3HT-NF solution was blended with a solvent (*m*-xylene)–diluted PDMS [10:1 (w/w) prepolymer/curing agent] to allow thorough mixing. A thin-film P3HT-NF/PDMS stretchable semiconductor is achieved by spin-coating, followed by solidifying at 60°C. We obtained the optimized weight composition of P3HT through systematic studies of the percolation behaviors, morphologies, and their electrical characteristics (fig. S3). The P3HT/PDMS weight ratio of 2:8 was chosen owing to the absence of microcracks and a moderate decrease in mobilities, as shown in fig. S4. We carried out AFM scanning to examine the microstructures

of the nanofibrils and the detailed surface morphology of the P3HT-NF/PDMS thin film spin-coated on a PDMS substrate. The left AFM image in Fig. 1D with a scanning area of 1 μm × 1 μm shows the surface topography of the film. The right AFM image in Fig. 1D under phase mode illustrates the stiffness contrast between P3HT-NFs (~0.3 GPa) (*31*) and PDMS (~1 MPa) (*32*). The schematic illustration in fig. S2E shows how the P3HT-NFs behave upon stretching at different extent. The P3HT-NFs first straighten and then eventually start to rupture, which can be seen from the AFM images in Fig. 1E. As the yellow arrows indicate, some P3HT-NFs rupture when stretched up to or beyond 50%. Nevertheless, majorities of the P3HT-NFs remain connected at 50%. Owing to the composite merits of elastomeric mechanical properties from the elastomer PDMS and the electrical conductance from the percolated P3HT-NFs, the P3HT-NF/PDMS can be stretched or twisted and return to its original state without any cracks, as shown in Fig. 1F. The stretchable ion gel dielectric was prepared by the solution-casting method. The detailed preparation can be found in Materials and Methods. The composite shows relatively stable electrical conductivity even after exposure in the environment (25°C, 75% relative humidity) for 600 hours (fig. S5). No obvious crack of the membrane was observed when it was stretched by 50%, as shown in Fig. 1G.

Intrinsically stretchable rubbery transistors

We constructed stretchable ion gel–gated TFTs by using these intrinsically stretchable electronic materials based on solution processes, including spin casting and stencil printing. Figure 2A shows the schematic structure of an ion gel–gated TFT. Specifically, the source and drain AuNP-AgNW/PDMS electrodes and P3HT-NF/PDMS composite semiconductor layer were patterned with a thin Kapton film–based stencil masks, which were generated by a cutting machine (Silhouette Cameo). A 140-μm-thick ion gel film was aligned and laminated on the source and drain electrodes to serve as ion-gated dielectric. The detailed fabrication process is described in Materials and Methods and fig. S6. Figure 2 (B and C) shows a photograph of fabricated TFT and an SEM image showing a channel length of 50 μm, respectively. The width of the channel was 5 mm. The thicknesses of the P3HT-NF/PDMS composite semiconductor and TFT were measured to be ~280 nm and ~430 μm, respectively (fig. S7).

To verify the necessity and feasibility of AuNP-AgNW/PDMS electrodes for the intrinsically stretchable rubbery TFT, we tested several different electrodes and carefully examined their corresponding characteristics. Specifically, we constructed TFTs and tested electron beam–evaporated Au and Ag electrodes and AgNW/PDMS– and AuNP-AgNW/PDMS–based electrodes. Only Au electrodes and AuNP-AgNW/PDMS–based TFTs showed transistor characteristics. The comparison results are presented in fig. S8. The results suggest that only Au or AuNP-AgNW can form an ohmic contact with the P3HT-NF/PDMS, and the Ag film or AgNW cannot (*28*).

Figure 2D shows the transfer $I_{ds} \sim V_G$ and corresponding $|I_{ds}|^{1/2} \sim V_G$ curves of the stretchable ion-gated TFT without any mechanical stretching. The drain current was obtained while the gate voltage (V_G) was swept from 0 to −4 V, with the drain voltage kept at −0.5 V. The $I_{ON/OFF}$ was calculated to be ~5.6×10^3, which is comparable to other P3HT-NF–based stretchable TFTs (*23*). Figure 2E shows the source-drain I_{DS}-V_{DS} characteristics of the TFT with a gate voltage decrease from −1.5 to −4 V at a voltage step of −0.5 V. The drain voltage was decreased from 0 to −0.5 V. The drain current was as high as ~0.35 mA at $V_G = -4$ V and $V_{DS} = -0.5$ V.

To verify that the TFTs from P3HT-NF/PDMS composite semiconductor can offer enhanced device performance, we construct TFTs with a semiconductor from pristine P3HT and PDMS (p-P3HT/PDMS) composite on Au electrodes as a comparison. The TFTs from p-P3HT/PDMS and P3HT-NF/PDMS composite showed μ_{FE} of 4.5×10^{-3} and 1.3 $cm^2/V{\cdot}s$ and $I_{ON/OFF}$ of 1.68×10^2 and 3.82×10^2, respectively. Details are illustrated in fig. S9. Compared to p-P3HT, P3HT-NFs obtained through π conjugation of the thiophene rings yielded more efficient carrier transport and better device performance. These results are also consistent with the reported P3HT-NF–based devices (*33*).

To examine the transistor performances under mechanical strain, the characteristics of the fabricated TFT were measured while different levels of mechanical strain were applied using a custom-made stretcher. The strain was applied both along and perpendicular to the channel length directions. Because the TFT was constructed fully with elastomeric materials whose moduli are comparable and thus with no significant strain isolation effect (*34*, *35*), the stretching strain applied is assumed to be evenly distributed across the whole device. Figure 2 (F and G) shows the transfer curves of the TFTs under 10, 30, and 50% mechanical strain along and perpendicular to the channel length directions, respectively. More detailed results are shown in fig. S10. On the basis of the linear regime of these transfer curves, the μ and threshold voltage (V_{th}) of the TFTs under different levels of mechanical strain were calculated (see the Supplementary Materials for details).

On one hand, once the TFT was stretched by up to 50% along the channel length direction, a moderate decrease in μ from 1.4 to 0.8 $cm^2/V{\cdot}s$ and a slight increase in V_{th} from −2.56 to −2.45 V were obtained (Fig. 2H). On the other hand, once it was stretched by up to 50% perpendicular to the channel length direction, a relatively larger decrease in μ from 1.4 to 0.4 $cm^2/V{\cdot}s$ and a slight decrease in V_{th} from −2.56 to −2.61 V were obtained (Fig. 2I). Note that owing to the gating effect, the TFT experiences less decrease in the channel current upon mechanical stretching compared with the devices without a gate, such as strain sensors, as described below. A similar phenomenon has been reported elsewhere (*36*). All these results suggest that the intrinsically stretchable rubbery transistors can maintain normal operation and relatively stable device performances while undergoing large mechanical stretching.

Strain, pressure, and temperature sensors

Various sensors, such as strain, pressure, and temperature sensors, were exploited by using intrinsically stretchable electronic materials. Figure 3A shows a schematic illustration of a strain sensor with a two-terminal configuration in which a P3HT-NF/PDMS stretchable semiconductor is connected at both ends with AuNP-AgNW/PDMS electrodes. The length and width of the channel were 50 μm and 5 mm, respectively. The thickness of the P3HT-NF/PDMS stretchable semiconductor was ~100 nm. The device was fabricated in a way similar to that of the transistor. Figure 3B presents a series of images of a device stretched from 0 to 50%. Upon stretching, the electrical resistance increases. Figure 3C shows the plot of the measured electrical resistance versus the mechanical strain from 0 to 50% for both directions. When the applied strain was along the channel length direction, the resistance increased from 0.3 to 4.6 gigohms, and an approximately linear increase of resistance was obtained upon mechanical stretching. Note that the increase of resistance was mainly attributed to the semiconductor rather than to the conductor. The conductor contributes negligibly, as exhibited in Fig. 1C, compared with the overall resistance increase.

When the applied strain was perpendicular to the channel length direction, a much smaller increase in resistance from 0.3 to 0.64 gigohms was observed. Cyclic mechanical stretching and releasing of the strain sensor under a cyclic mechanical tester (CK-700FET, CKSI Co. Ltd.)

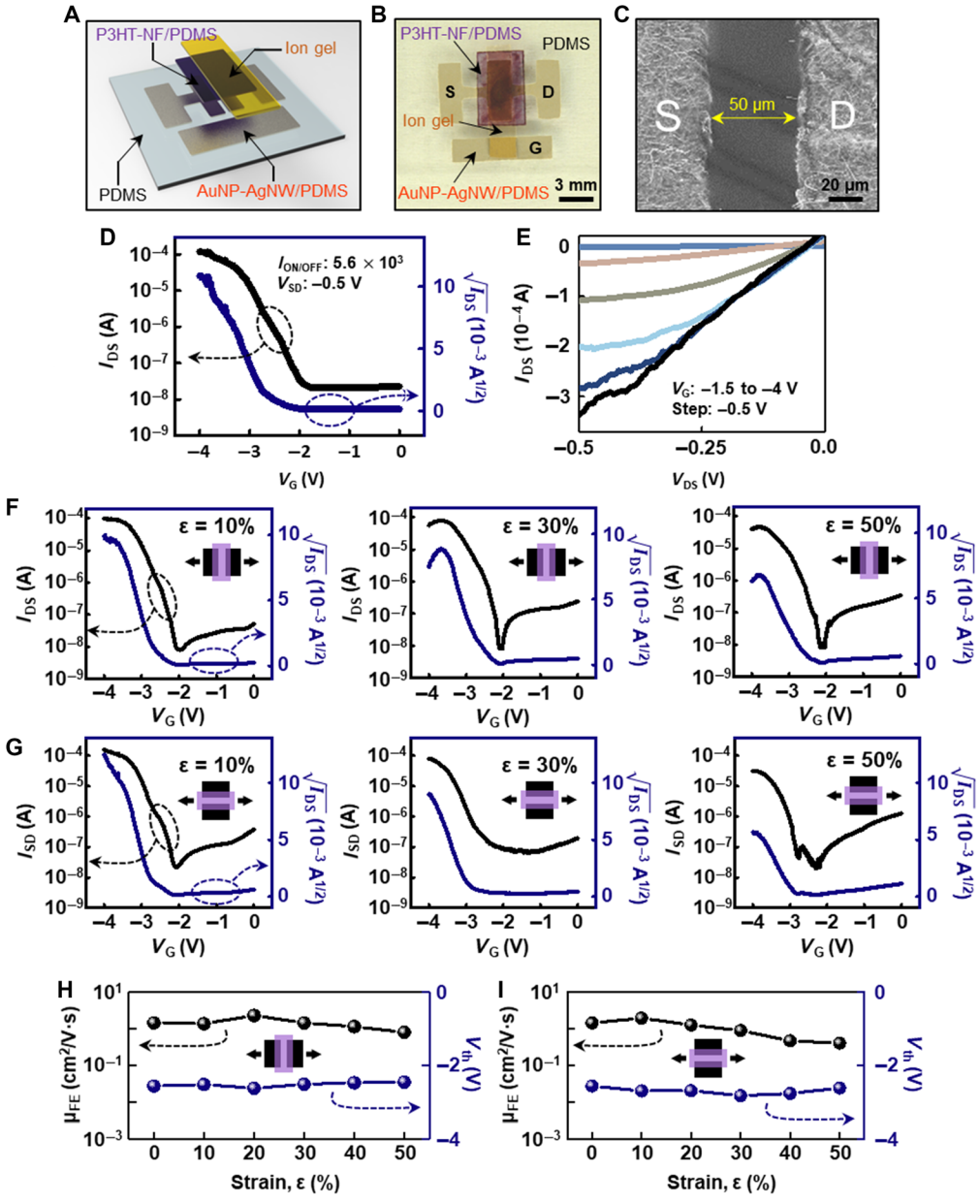

Fig. 2. Intrinsically stretchable rubbery transistors. (**A**) Exploded schematic illustration of the rubbery TFT. (**B**) Photograph of the TFT. (**C**) SEM image of the source, drain electrodes, and channel of the TFT. (**D** and **E**) Transfer and output curves of the TFT without any mechanical strain. (**F** and **G**) Transfer curves of the TFTs under different levels of mechanical strain along and perpendicular to the channel length directions. (**H** and **I**) μ_{FE} and V_{th} of the TFTs under different levels of mechanical strain along and perpendicular to the channel length directions.

were performed to evaluate the stability of the sensor. The stretching increased from 0 to 50%, with a step increase of 10% along the channel length direction. Figure 3D shows the normalized electrical resistance during cyclic stretching and releasing at a rate of 1 Hz. These results agree with the measured resistance change, as shown in Fig. 3C. The inset in Fig. 3D shows a magnified resistance change of the sensor at 30% cyclic stretching, and stable and repetitive response was achieved. The calculated gauge factor (GF), defined as the ratio between the relative resistance change ($\Delta R/R_o$) and the extent of mechanical stretching, is shown in Fig. 3E. A GF of 33 is achieved for the 50% stretching. Note that this GF value is the highest, to our best knowledge, compared with GF values of other organic material– and inorganic material–based strain sensors that can be directly stretched to a similar extent, such as 50% (*37*, *38*).

A similar two-terminal device configuration was adopted for pressure sensors because the applied pressure induces semiconductor deforming, which results in resistance change. Specifically, relative electrical resistance (R/R_o) was consecutively measured by applying different Hertzian contact pressures (see the Supplementary Materials for details). As shown in Fig. 3F, the applied pressure ranges from 0.66 to 1.2 MPa, and the resistance changes accordingly. With an increase of the applied Hertzian pressure from 0.66 to 1.2 MPa, the R/R_o increases from ~0.98 to ~3.3. The change of R/R_o corresponding to different applied pressures is plotted in Fig. 3G. The near hysteresis-less characteristic

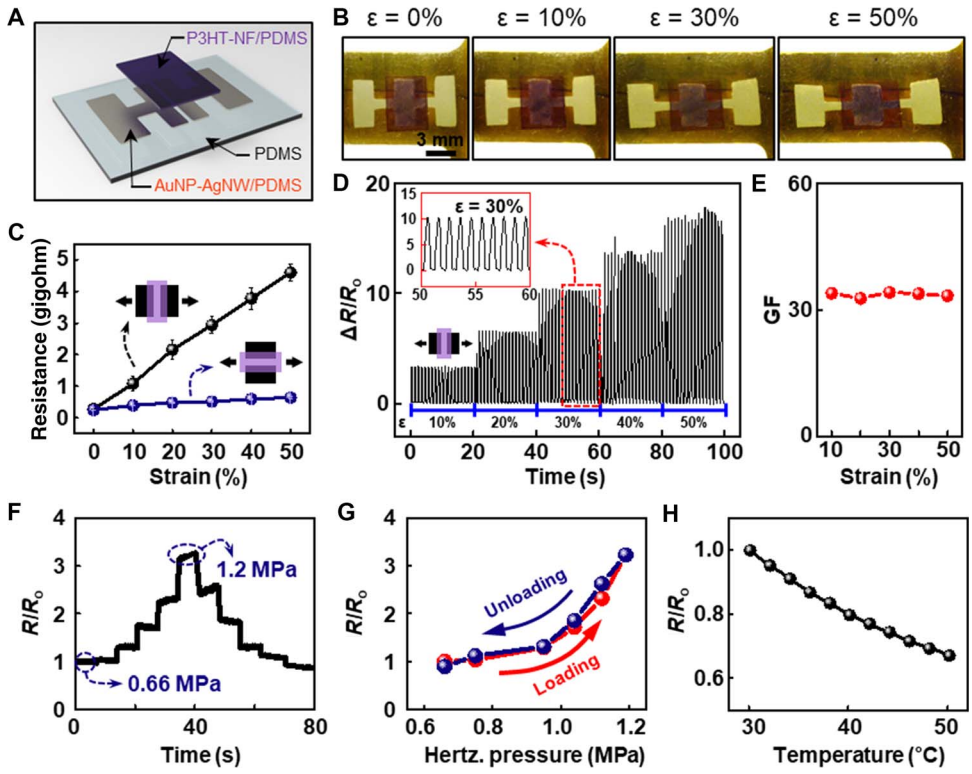

Fig. 3. Rubbery strain, pressure, and temperature sensors. (**A**) Exploded schematic illustration of the strain sensor. (**B**) Photographs of the sensors under different levels of mechanical strain. (**C**) Measured electrical resistance of the strain sensor under different levels of mechanical strain along the channel length direction (black) and perpendicular to the channel length direction (blue). (**D**) Relative change of the resistance ($\Delta R/R_o$) under cyclic stretching and releasing. (**E**) GF of the strain sensor with respect to the different strain. (**F**) Relative electrical resistance (R/R_o) change of the pressure sensor with respect to time under different levels of pressure. (**G**) Relative electrical resistance change of the pressure sensor under a loading (red) and unloading (blue) cycle. (**H**) Relative electrical resistance change of the temperature sensor with respect to the different temperature.

for the loading/unloading cycle suggests that this device is a viable pressure sensor.

Temperature sensors were also exploited with the similar two-terminal device structure. The resistance changes of R/R_o with respect to different temperatures were carefully examined. As shown in Fig. 3H, the R/R_o decreased from 1.0 to 0.67 with an increase of temperature from 30° to 50°C. The experienced resistivity decrease is a major result of increased carrier concentration, which agrees with the reported work on P3HT from others (*39*–*41*). The measured temperature coefficients of resistance at 303 K (30°C), 313 K (40°C), and 323 K (50°C) are −0.028/K, −0.023/K, and −0.016/K, respectively (see the Supplementary Materials for details).

Intrinsically stretchable rubbery sensors for robotic skins

Owing to the simple form of rubber, the merits of great stretchability, and the retention of electrical functions, we applied our intrinsically stretchable rubbery device methods to construct smart artificial skins for robot hands, in which large deformations exist locally near the joints. As a demonstration, Fig. 4A presents arrays of strain, pressure, and temperature sensors mounted on a robotic hand (Star Wars Science, Darth Vader robotic arm). In particular, the temperature and pressure sensors were placed on the phalanges instead of the joints of the fingers to avoid coupled output from the finger motions. This artificial skin is implemented to impart capabilities, such as gesture interpretation and haptic sensing for robots. Specifically, the strain sensors directly translate the gesture into an electrical parameter, that is, resistance, which will facilitate the understanding of sign language. The strain sensor characteristics were calibrated for the finger subjected to different bending angles, wherein different mechanical strains are associated. As exhibited in Fig. 4 (B and C), the electrical resistances are 0.50, 0.78, 0.98, 1.35, and 1.57 gigohms corresponding to angles of 0°, 30° (that is, ε = 8%), 45° (ε = 10%), 60° (ε = 13%), and 90° (ε = 15%), respectively. These results are consistent with the aforementioned results in Fig. 3D. Direct linkage between the mappings of the resistance of the deformed strain sensor array with the specific gestures of the sign language alphabet has been built. A whole set of finger-based gestures of the sign language alphabet can be translated into letters by using 14 strain sensors that are mounted on all the joints of a robot finger. For example, to express the sign language alphabet "Y", the index, middle, and ring fingers are completely folded (providing higher electrical resistance, >1.3 gigohms), whereas the thumb and pinky fingers were straightened (showing lower electrical resistance, <0.5 gigohms) (fig. S9). Figure 4D shows a set of letters, representing "YU LAB," which was translated by configuring the hand into specific gestures correspondingly. The details of the sign language translation can be found in the Supplementary Materials and figs. S11 and S12. Although the sensors have shown the capability of translating the majority of the gestures in American Sign Language, note that integrating these sensors with other types of devices, such as accelerometers, suggests a possible approach to differentiating the letters (for example, I and J) with similar gestures but different motions.

To demonstrate its use as a temperature sensor, the skin with temperature sensors implemented on the robot hand was in contact with

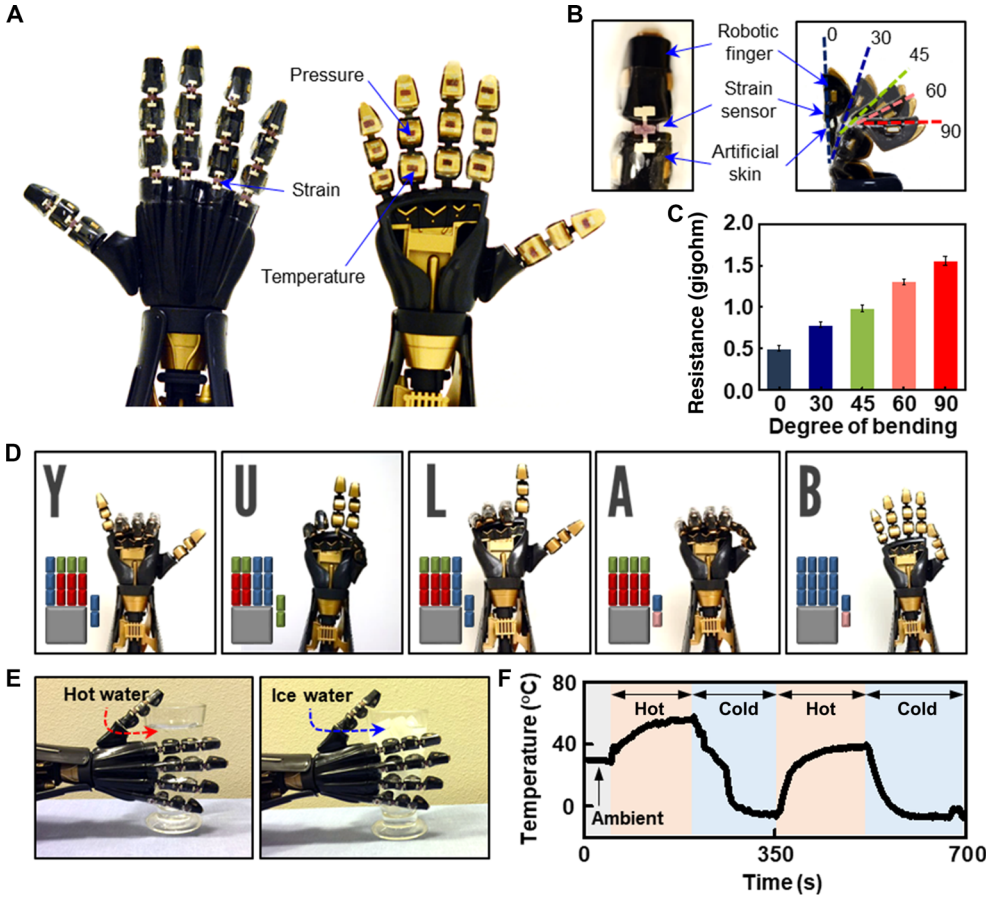

Fig. 4. Intrinsically stretchable rubbery electronics–based robotic skins. (**A**) Photographs of a robotic hand with intrinsically stretchable rubbery sensors. (**B**) Photograph of strain sensors located on the hinges of a robotic finger (left, top view) and overlapped photograph of the robotic finger with different bending angles from 0° to 90° (right, side view). (**C**) Electrical resistance of the strain sensor under different degrees of bending. (**D**) Demonstration of using an array of strain sensors on a robotic hand to translate sign language alphabets. The inset schematics of the colored hand are electrical resistance values that correspond to (C) for the corresponding hand gestures (see the Supplementary Materials and figs. S11 and S12 for details). (**E**) Photographs of the robotic hand with the temperature sensors touching hot (left) and cold (right) cups. (**F**) Measured sensor responses while the hand with skin touched the hot and cold cups alternatively.

a cup filled with hot and cold (ice) water alternatively, as shown in Fig. 4E. The measured temperature response for two cycles of touching the hot and cold cup is shown in Fig. 4F. Governed by the geometries and materials of the skin and robot hand, the rise time (that is, the time required for the temperature to rise to 90% of its final temperature) is about 80 s and the fall time (that is, the time required for the temperature to fall to 10% of its final temperature) is about 50 s. Note that the speed of thermal response can be potentially improved through an amended thermal system, optimized geometries of the sensors, and enhanced thermal conductivity of the composites through inclusion of additives (such as graphene and carbon nanotubes).

DISCUSSION

The elastomeric composite semiconductors and conductors in this work enable a class of stretchable electronics and sensors that are intrinsically highly stretchable without any requirement for additional mechanical structure designs for traditional nonstretchable semiconductors. The elastomeric composite semiconductor of P3HT-NF/PDMS can all be created from common and commercially available materials. We demonstrate that stretchable electronics and sensors can also be created with simple fabrication steps by using these stretchable electronic materials. Our results show that intrinsically stretchable transistors remain functional while stretched by 50% and the elastomeric composite semiconductor achieves very high mobility while moderate mobility decrease is observed, that the strain sensors operate in a stable manner while achieving the highest GF for large level strains, that the pressure and temperature sensors show reliable performances, and that the intrinsically stretchable electronics and sensors can be used as smart skins for robotics. We foresee that this strategy of enabling elastomeric semiconductors by percolating semiconductor nanofibrils into a rubber will advance the development of stretchable semiconductors, and the approach to constructing electronics and sensors all from elastomeric electronic materials will move forward the advancement of stretchable electronics for a wide range of applications, such as artificial skins, biomedical implants, and surgical gloves.

MATERIALS AND METHODS

Materials

Anhydrous *m*-xylene (>99%), acetone (>99.9%), regioregular P3HT (rr-P3HT), poly(vinylidene fluoride-*co*-hexafluoropropylene) (PVDF-HFP;

M_w ~400,000), 1-ethyl-3-methylimidazolium trifluoromethanesulfonate (EMIM-Otf; >98%), gold chloride trihydrate (>99.9%), and anhydrous ammonia (28%) were all from Sigma-Aldrich and used as received. AgNW (~99.5%) solution (average diameter and length are 120 nm and 20 μm, respectively) was from ACS Material.

Fabrication of elastomeric composite conductor

The fabrication of the conductor involves generating patterned AgNWs, embedding them into PDMS to form stretchable structures, and coating them with AuNPs using a galvanic replacement process. To pattern the electrodes, we first manufactured a shadow mask of 25-μm-thick Kapton film using a programmable cutting machine (Silhouette Cameo). AgNW solution (15 mg/ml) was drop-casted on a precleaned glass with the shadow mask and dried for 10 min at 60°C. The samples were then heated on a hot plate for 30 min at 200°C to enhance their electrical conductivity. A PDMS solution [10:1 (w/w) prepolymer/curing agent] was spin-coated on the patterned AgNWs at 300 rpm for 60 s followed by curing for 4 hours at 60°C to solidify. The PDMS was then peeled off from the glass to obtain patterned AgNWs embedded in PDMS. Owing to the high viscosity of the PDMS solution, this process results in AgNWs partially embedded within the PDMS. To coat the exposed AgNWs with AuNPs, the AgNW/PDMS sample was immersed in 0.5 mM $HAuCl_4 \cdot H_2O$ aqueous solution for 2 min for the Ag-Au replacement process and dipped in NH_4OH solution (28%) for 1 min to dissolve AgCl layers that were formed on the NWs. The fabrication of elastomeric conductor was completed by rinsing in water and drying with a N_2 gun.

Fabrication of ion gel dielectric

The ion gel dielectric solution was prepared by blending PVDF-HFP, ionic liquid EMIM-Otf, and acetone at a weight ratio of 1:4:7 at 70°C. The ion gel membrane was achieved by casting the solution on a precleaned glass and cured to solidify under vacuum for 12 hours at 70°C (*42*, *43*). The solidified membrane can be easily cut into different shapes and picked up from the glass (*43*). The capacitance of ion gel, which was obtained using an LCR meter (U1252B, Keysight) and an oscilloscope (DSO-X 2004A, Agilent), was 9.8 $\mu F/cm^2$ at 1 kHz, in agreement with the values in the literature (*43*–*45*).

Fabrication of stretchable TFTs

The fabrication of the TFTs involved generating source and drain electrodes, forming a thin-film composite semiconductor, and laminating the ion gel dielectric. The source and drain electrodes were fabricated in a way similar to that of the elastomeric conductor, as described before. A Kapton shadow mask was used to pattern the P3HT-NF/PDMS composite semiconductor. After the shadow mask was aligned and laminated on the electrodes, the P3HT-NF/PDMS solution was spin-coated at 2000 rpm for 60 s and dried for 30 min at 90°C. The patterned semiconductor film was achieved by carefully removing the shadow mask. Finally, a piece of the 140-μm-thick ion gel with different planar geometries was aligned and laminated on the device as a dielectric.

Characterization of stretchable electronic materials and devices

The surface morphology of the composite semiconductor was characterized using an AFM (Veeco Dimension 3000) under the tapping mode. The SEM (XL-30S FEG, Philips) and TEM (JEM-2010, JEOL Ltd.) images were taken to examine the microstructures of the electronic materials. The *I*-*V* characteristics of the devices were measured by using a probe station (H100, Signatone) equipped with a semiconductor characterization system (4200-SCS, Keithley Instruments Inc.). Cyclic mechanical stretching and releasing tests were performed by using an IPC flexural endurance tester (CK-700FET, CKSI Co. Ltd.).

SUPPLEMENTARY MATERIALS

Supplementary material for this article is available at http://advances.sciencemag.org/cgi/content/full/3/9/e1701114/DC1

Calculation of μ_{FE} and V_{th}

Optimized P3HT weight composition in P3HT-NF/PDMS composites

Calculation of temperature coefficient of resistance

Calculation of Hertzian contact pressure

Sign language translation program

fig. S1. Fabrication of AuNP-AgNW by using a galvanic replacement process.

fig. S2. Fabrication and deformed states of the elastomeric composite semiconductor.

fig. S3. Percolation behavior of the P3HT-NF/PDMS composite semiconductor.

fig. S4. The composites with different weight compositions of P3HT and PDMS.

fig. S5. Lifetime of the elastomeric composite conductor and semiconductor.

fig. S6. Fabrication steps of the intrinsically stretchable TFTs and sensors.

fig. S7. Thickness of the rubbery TFT and P3HT-NF/PDMS semiconductor composite.

fig. S8. P3HT-NF/PDMS composite–based TFTs with different electrodes.

fig. S9. Performances of TFTs based on p-P3HT/PDMS and P3HT-NF/PDMS as semiconducting channels.

fig. S10. TFT performances with respect to mechanical strain.

fig. S11. Electrical resistance response of the strain sensor under a given hand gesture.

fig. S12. The sign language translation program.

References (*46*, *47*)

REFERENCES AND NOTES

1. A. Koh, D. Kang, Y. Xue, S. Lee, R. M. Pielak, J. Kim, T. Hwang, S. Min, A. Banks, P. Bastien, M. C. Manco, L. Wang, K. R. Ammann, K.-I. Jang, P. Won, S. Han, R. Ghaffari, U. Paik, M. J. Slepian, G. Balooch, Y. Huang, J. A. Rogers, A soft, wearable microfluidic device for the capture, storage, and colorimetric sensing of sweat. *Sci. Transl. Med.* **8**, 366ra165 (2016).
2. T. Yokota, P. Zalar, M. Kaltenbrunner, H. Jinno, N. Matsuhisa, H. Kitanosako, Y. Tachibana, W. Yukita, M. Koizumi, T. Someya, Ultraflexible organic photonic skin. *Sci. Adv.* **2**, e1501856 (2016).
3. S. I. Park, D. S. Brenner, G. Shin, C. D. Morgan, B. A. Copits, H. U. Chung, M. Y. Pullen, K. N. Noh, S. Davidson, S. J. Oh, J. Yoon, K.-I. Jang, V. K. Samineni, M. Norman, J. G. Grajales-Reyes, S. K. Vogt, S. S. Sundaram, K. M. Wilson, J. S. Ha, R. Xu, T. Pan, T.-i. Kim, Y. Huang, M. C. Montana, J. P. Golden, M. R. Bruchas, R. W. Gereau IV, J. A. Rogers, Soft, stretchable, fully implantable miniaturized optoelectronic systems for wireless optogenetics. *Nat. Biotechnol.* **33**, 1280–1286 (2015).
4. H. Fang, K. J. Yu, C. Gloschat, Z. Yang, E. Song, C.-H. Chiang, J. Zhao, S. M. Won, S. Xu, M. Trumpis, Y. Zhong, S. W. Han, Y. Xue, D. Xu, S. W. Choi, G. Cauwenberghs, M. Kay, Y. Huang, J. Viventi, I. R. Efimov, J. A. Rogers, Capacitively coupled arrays of multiplexed flexible silicon transistors for long-term cardiac electrophysiology. *Nat. Biomed. Eng.* **1**, 0038 (2017).
5. L. Xu, S. R. Gutbrod, A. P. Bonifas, Y. Su, M. S. Sulkin, N. Lu, H.-J. Chung, K.-I. Jang, Z. Liu, M. Ying, C. Lu, R. C. Webb, J.-S. Kim, J. I. Laughner, H. Cheng, Y. Liu, A. Ameen, J.-W. Jeong, G.-T. Kim, Y. Huang, I. R. Efimov, J. A. Rogers, 3D multifunctional integumentary membranes for spatiotemporal cardiac measurements and stimulation across the entire epicardium. *Nat. Commun.* **5**, 3329 (2014).
6. H.-H. Chou, A. Nguyen, A. Chortos, J. W. F. To, C. Lu, J. Mei, T. Kurosawa, W.-G. Bae, J. B.-H. Tok, Z. Bao, A chameleon-inspired stretchable electronic skin with interactive colour changing controlled by tactile sensing. *Nat. Commun.* **6**, 8011 (2015).
7. J. Kim, M. Lee, H. J. Shim, R. Ghaffari, H. R. Cho, D. Son, Y. H. Jung, M. Soh, C. Choi, S. Jung, K. Chu, D. Jeon, S.-T. Lee, J. H. Kim, S. H. Choi, T. Hyeon, D.-H. Kim, Stretchable silicon nanoribbon electronics for skin prosthesis. *Nat. Commun.* **5**, 5747 (2014).
8. J. Kim, G. A. Salvatore, H. Araki, A. M. Chiarelli, Z. Xie, A. Banks, X. Sheng, Y. Liu, J. W. Lee, K.-I. Jang, S. Y. Heo, K. Cho, H. Luo, B. Zimmerman, J. Kim, L. Yan, X. Feng, S. Xu, M. Fabiani, G. Gratton, Y. Huang, U. Paik, J. A. Rogers, Battery-free, stretchable optoelectronic systems for wireless optical characterization of the skin. *Sci. Adv.* **2**, e1600418 (2016).
9. Y. Liu, J. J. S. Norton, R. Qazi, Z. Zou, K. R. Ammann, H. Liu, L. Yan, P. L. Tran, K.-I. Jang, J. W. Lee, D. Zhang, K. A. Kilian, S. H. Jung, T. Bretl, J. Xiao, M. J. Slepian, Y. Huang, J.-W. Jeong, J. A. Rogers, Epidermal mechano-acoustic sensing electronics for cardiovascular diagnostics and human-machine interfaces. *Sci. Adv.* **2**, e1601185 (2016).

10. S. Lee, Y. Inoue, D. Kim, A. Reuveny, K. Kuribara, T. Yokota, J. Reeder, M. Sekino, T. Sekitani, Y. Abe, T. Someya, A strain-absorbing design for tissue–machine interfaces using a tunable adhesive gel. *Nat. Commun.* **5**, 5898 (2014).
11. T. Q. Trung, N.-E. Lee, Recent progress on stretchable electronic devices with intrinsically stretchable components. *Adv. Mater.* **29**, 1603167 (2017).
12. T. Q. Trung, N.-E. Lee, Materials and devices for transparent stretchable electronics. *J. Mater. Chem. C* **5**, 2202–2222 (2017).
13. M. Kaltenbrunner, T. Sekitani, J. Reeder, T. Yokota, K. Kuribara, T. Tokuhara, M. Drack, R. Schwödiauer, I. Graz, S. Bauer-Gogonea, S. Bauer, T. Someya, An ultra-lightweight design for imperceptible plastic electronics. *Nature* **499**, 458–463 (2013).
14. C. Dagdeviren, Y. Shi, P. Joe, R. Ghaffari, G. Balooch, K. Usgaonkar, O. Gur, P. L. Tran, J. R. Crosby, M. Meyer, Y. Su, R. Chad Webb, A. S. Tedesco, M. J. Slepian, Y. Huang, J. A. Rogers, Conformal piezoelectric systems for clinical and experimental characterization of soft tissue biomechanics. *Nat. Mater.* **14**, 728–736 (2015).
15. S. Xu, Z. Yan, K.-I. Jang, W. Huang, H. Fu, J. Kim, Z. Wei, M. Flavin, J. McCracken, R. Wang, A. Badea, Y. Liu, D. Xiao, G. Zhou, J. Lee, H. U. Chung, H. Cheng, W. Ren, A. Banks, X. Li, U. Paik, R. G. Nuzzo, Y. Huang, Y. Zhang, J. A. Rogers, Assembly of micro/nanomaterials into complex, three-dimensional architectures by compressive buckling. *Science* **347**, 154–159 (2015).
16. S. Xu, Y. Zhang, J. Cho, J. Lee, X. Huang, L. Jia, J. A. Fan, Y. Su, J. Su, H. Zhang, H. Cheng, B. Lu, C. Yu, C. Chuang, T.-i. Kim, T. Song, K. Shigeta, S. Kang, C. Dagdeviren, I. Petrov, P. V. Braun, Y. Huang, U. Paik, J. A. Rogers, Stretchable batteries with self-similar serpentine interconnects and integrated wireless recharging systems. *Nat. Commun.* **4**, 1543 (2013).
17. M. Isobe, K. Okumura, Initial rigid response and softening transition of highly stretchable kirigami sheet materials. *Sci. Rep.* **6**, 24758 (2016).
18. A. Lamoureux, K. Lee, M. Shlian, S. R. Forrest, M. Shtein, Dynamic kirigami structures for integrated solar tracking. *Nat. Commun.* **6**, 8092 (2015).
19. T. C. Shyu, P. F. Damasceno, P. M. Dodd, A. Lamoureux, L. Xu, M. Shlian, M. Shtein, S. C. Glotzer, N. A. Kotov, A kirigami approach to engineering elasticity in nanocomposites through patterned defects. *Nat. Mater.* **14**, 785–789 (2015).
20. J. Liang, L. Li, D. Chen, T. Hajagos, Z. Ren, S.-Y. Chou, W. Hu, Q. Pei, Intrinsically stretchable and transparent thin-film transistors based on printable silver nanowires, carbon nanotubes and an elastomeric dielectric. *Nat. Commun.* **6**, 7647 (2015).
21. S. Yao, Y. Zhu, Nanomaterial-enabled stretchable conductors: Strategies, materials and devices. *Adv. Mater.* **27**, 1480–1511 (2015).
22. M. Shin, J. Y. Oh, K.-E. Byun, Y.-J. Lee, B. Kim, H.-K. Baik, J.-J. Park, U. Jeong, Polythiophene nanofibril bundles surface-embedded in elastomer: A route to a highly stretchable active channel layer. *Adv. Mater.* **27**, 1255–1261 (2015).
23. E. Song, B. Kang, H. H. Choi, D. H. Sin, H. Lee, W. H. Lee, K. Cho, Stretchable and transparent organic semiconducting thin film with conjugated polymer nanowires embedded in an elastomeric matrix. *Adv. Electron. Mater.* **2**, 1500250 (2016).
24. M. Shin, J. H. Song, G.-H. Lim, B. Lim, J.-J. Park, U. Jeong, Highly stretchable polymer transistors consisting entirely of stretchable device components. *Adv. Mater.* **26**, 3706–3711 (2014).
25. A. Chortos, J. Lim, J. W. F. To, M. Vosgueritchian, T. J. Dusseault, T.-H. Kim, S. Hwang, Z. Bao, Highly stretchable transistors using a microcracked organic semiconductor. *Adv. Mater.* **26**, 4253–4259 (2014).
26. J. Y. Oh, S. Rondeau-Gagné, Y.-C. Chiu, A. Chortos, F. Lissel, G.-J. N. Wang, B. C. Schroeder, T. Kurosawa, J. Lopez, T. Katsumata, J. Xu, C. Zhu, X. Gu, W.-G. Bae, Y. Kim, L. Jin, J. W. Chung, J. B.-H. Tok, Z. Bao, Intrinsically stretchable and healable semiconducting polymer for organic transistors. *Nature* **539**, 411–415 (2016).
27. J. Xu, S. Wang, G.-J. N. Wang, C. Zhu, S. Luo, L. Jin, X. Gu, S. Chen, V. R. Feig, J. W. F. To, S. Rondeau-Gagné, J. Park, B. C. Schroeder, C. Lu, J. Y. Oh, Y. Wang, Y.-H. Kim, H. Yan, R. Sinclair, D. Zhou, G. Xue, B. Murmann, C. Linder, W. Cai, J. B.-H. Tok, J. W. Chung, Z. Bao, Highly stretchable polymer semiconductor films through the nanoconfinement effect. *Science* **355**, 59–64 (2017).
28. M.-Y. Chuang, H.-W. Zan, P. Yu, Y.-C. Lai, H.-F. Meng, Gas permeable silver nanowire electrode for realizing vertical type sensitive gas sensor. *Org. Electron.* **15**, 2769–2774 (2014).
29. H. Lee, S. Hong, J. Lee, Y. D. Suh, J. Kwon, H. Moon, H. Kim, J. Yeo, S. H. Ko, Highly stretchable and transparent supercapacitor by Ag–Au core–shell nanowire network with high electrochemical stability. *ACS Appl. Mater. Interfaces* **8**, 15449–15458 (2016).
30. Y. Lee, J. Y. Oh, S. Y. Son, T. Park, U. Jeong, Effects of regioregularity and molecular weight on the growth of polythiophene nanofibrils and mixes of short and long nanofibrils to enhance the hole transport. *ACS Appl. Mater. Interfaces* **7**, 27694–27702 (2015).
31. D. Rodriquez, J.-H. Kim, S. E. Root, Z. Fei, P. Boufflet, M. Heeney, T.-S. Kim, D. J. Lipomi, Comparison of methods for determining the mechanical properties of semiconducting polymer films for stretchable electronics. *ACS Appl. Mater. Interfaces* **9**, 8855–8862 (2017).
32. R. Seghir, S. Arscott, Extended PDMS stiffness range for flexible systems. *Sens. Actuators A Phys.* **230**, 33–39 (2015).
33. M. Park, J.-S. Park, I. K. Han, J. Y. Oh, High-performance flexible and air-stable perovskite solar cells with a large active area based on poly(3-hexylthiophene) nanofibrils. *J. Mater. Chem. A* **4**, 11307–11316 (2016).
34. D.-H. Kim, Y.-S. Kim, J. Wu, Z. Liu, J. Song, H.-S. Kim, Y. Y. Huang, K.-C. Hwang, J. A. Rogers, Ultrathin silicon circuits with strain-isolation layers and mesh layouts for high-performance electronics on fabric, vinyl, leather, and paper. *Adv. Mater.* **21**, 3703–3707 (2009).
35. R.-H. Kim, D.-H. Kim, J. Xiao, B. H. Kim, S.-I. Park, B. Panilaitis, R. Ghaffari, J. Yao, M. Li, Z. Liu, V. Malyarchuk, D. G. Kim, A.-P. Le, R. G. Nuzzo, D. L. Kaplan, F. G. Omenetto, Y. Huang, Z. Kang, J. A. Rogers, Waterproof AlInGaP optoelectronics on stretchable substrates with applications in biomedicine and robotics. *Nat. Mater.* **9**, 929–937 (2010).
36. L. Zhou, S. Jung, E. Brandon, T. N. Jackson, Flexible substrate micro-crystalline silicon and gated amorphous silicon strain sensors. *IEEE Trans. Electron Devices* **53**, 380–385 (2006).
37. S. Savagatrup, E. Chan, S. M. Renteria-Garcia, A. D. Printz, A. V. Zaretski, T. F. O'Connor, D. Rodriquez, E. Valle, D. J. Lipomi, Plasticization of PEDOT: PSS by common additives for mechanically robust organic solar cells and wearable sensors. *Adv. Funct. Mater.* **25**, 427–436 (2015).
38. S.-H. Bae, Y. Lee, B. K. Sharma, H.-J. Lee, J.-H. Kim, J.-H. Ahn, Graphene-based transparent strain sensor. *Carbon* **51**, 236–242 (2013).
39. Y. Xia, J. H. Cho, J. Lee, P. P. Ruden, C. D. Frisbie, Comparison of the mobility–carrier density relation in polymer and single-crystal organic transistors employing vacuum and liquid gate dielectrics. *Adv. Mater.* **21**, 2174–2179 (2009).
40. W. F. Pasveer, J. Cottaar, C. Tanase, R. Coehoorn, P. A. Bobbert, P. W. M. Blom, D. M. de Leeuw, M. A. J. Michels, Unified description of charge-carrier mobilities in disordered semiconducting polymers. *Phys. Rev. Lett.* **94**, 206601 (2005).
41. B. D. Paulsen, C. D. Frisbie, Dependence of conductivity on charge density and electrochemical potential in polymer semiconductors gated with ionic liquids. *J. Phys. Chem. C* **116**, 3132–3141 (2012).
42. A. Sekiguchi, F. Tanaka, T. Saito, Y. Kuwahara, S. Sakurai, D. N. Futaba, T. Yamada, K. Hata, Robust and soft elastomeric electronics tolerant to our daily lives. *Nano Lett.* **15**, 5716–5723 (2015).
43. K. H. Lee, M. S. Kang, S. Zhang, Y. Gu, T. P. Lodge, C. D. Frisbie, "Cut and Stick" rubbery ion gels as high capacitance gate dielectrics. *Adv. Mater.* **24**, 4457–4462 (2012).
44. J. Lee, M. J. Panzer, Y. He, T. P. Lodge, C. D. Frisbie, Ion gel gated polymer thin-film transistors. *J. Am. Chem. Soc.* **129**, 4532–4533 (2007).
45. J. H. Cho, J. Lee, Y. Xia, B. Kim, Y. He, M. J. Renn, T. P. Lodge, C. D. Frisbie, Printable ion-gel gate dielectrics for low-voltage polymer thin-film transistors on plastic. *Nat. Mater.* **7**, 900–906 (2008).
46. Y. An, B. Y. Joo, D.-T. Chung, H. Kang, Finite element simulation of brittle fracture of bulletproof glass system. *Appl. Mech. Mater.* **566**, 468–473 (2014).
47. K. L. Johnson, *Contact Mechanics* (Cambridge Univ. Press, 1987).

Acknowledgments

Funding: C.Y. acknowledges the partial financial support from the NSF (ECCS-1509763 and CMMI-1554499), the Doctoral New Investigator grant from the American Chemical Society Petroleum Research Fund, and the Bill D. Cook faculty scholarship support from the Department of Mechanical Engineering at the University of Houston. **Author contributions:** H.-J.K. and C.Y. conceived and designed the experiments. H.-J.K., K.S., and A.T. performed the experiments. H.-J.K. and C.Y. analyzed the data. H.-J.K. and C.Y. wrote the paper. **Competing interests:** The authors declare that they have no competing interests. **Data and materials availability:** All data needed to evaluate the conclusions in the paper are present in the paper and/or the Supplementary Materials. Additional data related to this paper may be requested from the authors.

Submitted 10 April 2017
Accepted 9 August 2017
Published 8 September 2017
10.1126/sciadv.1701114

Citation: H.-J. Kim, K. Sim, A. Thukral, C. Yu, Rubbery electronics and sensors from intrinsically stretchable elastomeric composites of semiconductors and conductors. *Sci. Adv.* **3**, e1701114 (2017).